H_2 oxidation as criterion for PrOx catalyst selection: examples based on Au-CoO_x supported systems

Tomás Ramírez Reina, Cristina Megías-Sayago, Alejandro Pérez Florez, Svetlana Ivanova, Miguel Ángel Centeno, José Antonio Odriozola.

Departamento de Química Inorgánica e Instituto de Ciencia de Materiales de Sevilla, Centro mixto Universidad de Sevilla-CSIC, Avda. Américo Vespucio 49, 41092 Sevilla, Spain.

corresponding author: tomas.ramirez@icmse.csic.es

Abstract

A new approach for understanding PrOx reaction over gold catalysts is proposed in this work. The competition between H_2 and CO oxidation has been studied over a series of Au/CeO_2/Al_2O_3 and Au/CeO_2-CoO_x/Al_2O_3 catalysts in a simulated post-reforming gas stream for H_2 clean up goals containing H_2O and CO_2. The catalyst's behavior is correlated to their oxygen storage capacity, redox behavior and oxidation ability. The possible use of the hydrogen oxidation as a catalyst selection criterion is discussed.

Keywords: gold catalysts, H_2 oxidation, CO removal, PrOx.

1. Introduction

One of the most important issues related to the hydrogen technology is its difficulty to on board storage and distribution from a centralized production facility [1]. As a result, many efforts have been focused on the conversion of more readily available fuels to hydrogen, either for on board or for stationary applications. The hydrogen is mainly produced by hydrocarbons or alcohols reforming [2]. The reforming streams produce hydrogen accompanied by relatively high levels of carbon oxides and steam [1, 3].

An essential requisite for fueling the polyelectrolyte membrane fuel cells (PEMFC) with hydrogen is the absence of CO or at least its presence within the ultra-low trace levels, preferably less than 10 ppm. Therefore, CO abatement processes must be applied to reduce its levels in the H_2 stream. These purification processes are commonly composed by a combination of high- and low-temperature water gas shift reactions, allowing CO decrease to 1–2% level [4–6] and the preferential oxidation with air of the pre-cleaned reformate (PrOx) as a cheap and effective solution for the final purification step, since the range of working temperature matches that of the PEM fuel cells operation [7].

For PrOx reaction, the gold based catalysts are potentially advantageous [8, 9]. Earlier studies on Au/ceria catalysts found high activity and good selectivity of those systems in the 70–120 ºC temperature range, caused by the active participation of ceria in the oxidation process [10-12]. It is often reported that the presence of structural defects in the ceria lattice, e.g. oxygen vacancies, potentiates the activity of the gold based catalyst in the CO oxidation reaction [9, 13]. As a common strategy, the inclusion of heterocations in the ceria lattice is employed to increase the number of those defects [13-16]. The CO oxidation activity is then directly related to the concentration of those defects in such a way that; higher the number of defects, greater the oxygen mobility and higher the oxidation activity.

However, the above mentioned systems, together with the high efficiency in the CO oxidation possess limited selectivity due to their ability to burn H_2 with the same facility. As a result, any possible future application will be questioned by the selectivity more than by the activity. It is essential then to study the selectivity of the PrOx catalysts with the consideration of the H_2 oxidation, as a separate process. Several authors have studied H_2 oxidation and also the effect of H_2 presence on the selective CO oxidation on gold catalysts with contradictory results [17-20]. An enhancement of the CO oxidation activity in the presence of hydrogen was found in some studies [17, 19] and negative effect was reported by others [18, 20]. Notwithstanding the valuable information that can be extracted from these works, the influence of the realistic reforming streams e.g. the presence of H_2O and CO_2 and its effect on the hydrogen combustion were obviated. This major topic and some other questions, like, *which is the role of the support in the H_2 oxidation? Is there a support-dependent hydrogen effect on the CO oxidation? Are the gold nanoparticles the only responsible of the hydrogen oxidation?* remain unclear.

In order to address these issues, the main goal of this work is to study the hydrogen combustion and PrOx activity in presence of CO_2 and H_2O over gold based catalysts series. The H_2 oxidation have been taken as a criteria for providing clues directed toward the proper catalyst design and selection.

2. Experimental

2.1 Catalyst preparation

Support preparation

The supports were synthesized by a conventional impregnation method. The necessary amounts of metal precursor (cobalt and/or cerium nitrate, Aldrich) were impregnated on γ-alumina powder (Sasol). The impregnation was carried out in 50 mL of ethanol, evaporated till obtaining a dry solid in rotary vapour at reduced pressure and temperature of 50ºC. The resulting solid was then treated with NH_3 solution (10 $mol.L^{-1}$) during 30 min in order to assure the full conversion of the nitrates to hydroxides. The support was then filtered, dried and calcined at 500ºC for 4 hours. The fraction of 100-200 μm was retained for the gold deposition process.

Cerium or cobalt spinel oxide amount was fixed to 15 wt.% in the case of binary supports. For the ternary Al_2O_3 supported cerium-cobalt mixed oxides, 1 and 2 wt.% of Co_3O_4 loadings were fixed and corresponds to 0.067 and 0.134 Co/Ce molar ratio, respectively. In the adopted nomenclature the oxygen is omitted for simplification and the dopant contents are expressed as the corresponding theoretical loadings. For example, the CeCo2/Al solid should contain 15 wt.% cerium oxide and 2 wt.%. of Co_3O_4 both deposited on Al_2O_3.

Gold deposition

The gold (2 wt. % nominal value) was deposited by the direct anionic exchange method, assisted by NH_3 as described elsewhere [21]. The used Au precursor was $HAuCl_4$ (Alfa Aesar). After Au deposition the solid was dried in an oven at 100 °C overnight and calcined in air at 350°C for 4 h.

2.2 Characterization

The chemical composition of the samples was determined by X-Ray microfluorescence spectrometry (XRMF) in an EDAX Eagle III spectrophotometer with a rhodium source of radiation working at 40 KV.

X-ray diffraction (XRD) analysis was performed on an X'Pert Pro PANalytical. Diffraction patterns were recorded with Cu Kα radiation (40 mA, 45 kV) over a 2θ-range of 10 to 80º and a position-sensitive detector using a step size of 0.05º and a step time of 240 s.

High-Resolution Transmission Electron Microscopy (HRTEM) and High-Angle Annular Dark Field-Scanning Transmission Electron Microscopy (HAADF-STEM) images were recorded on a JEOL2010F instrument. The spatial resolution at Scherzer defocus conditions in HRTEM mode is 0.19 nm, while the HAADF-STEM studies were performed using an electron probe of 0.5 nm of diameter and a diffraction camera length of 10 cm.

The UV-Vis spectra were recorded on a Varian spectrometer model Cary 100, equipped with integrating sphere and using $BaSO_4$ as reference. All the spectra were collected in a diffuse reflectance mode and transformed to a magnitude proportional to the extinction coefficient through the Kubelka-Munk function F(α).

H_2-TPR was carried out in conventional U-shaped reactor as a function of temperature with a constant heating rate of 10 ºC.min^{-1} till 900 ºC over 50 mg of sample. 50 mL.min^{-1} certified 5%H_2 in Ar gas mixture was used and the H_2 consumption was followed by TCD detector and compared to that of CuO standard (99,999%).

For the Oxygen Storage Complete Capacity (OSCC) measurements, 100 mg of sample were loaded into a U-shaped quartz reactor and the temperature was raised in a 5%O_2/He flow (50 mL.min^{-1}) until 350 ºC with 10 ºC. min^{-1} heating rate. The system was then cooled and the temperature stabilized at the desired value in Ar flow (50 mL.min^{-1}). Then, ten O_2 pulses of 1 mL each were injected every 2 min. After 10 min of inert gas flow, ten H_2 pulses (1 mL each) were sent to saturate the surface with H_2 in order to reproduce as far as possible the PrOx reaction conditions. In the next step, after 10 min in inert gas flow, the samples were submitted to ten CO pulses (1 mL each). Again the sample is degassed during 10 min in Ar flow and subjected to new series of oxidizing pulses (10 O_2 pulses, 1mL) followed by five alternating pair of pulses (CO–O_2) permitting the determination of the Oxygen Storage Capacity (OSC) by the amount of CO_2 produced after the first CO alternated pulse. This methodology was employed at three different temperatures and the gas composition at the exit of the reactor was analyzed by a mass spectrometer PFEIFFER Vacuum PrismaPlus controlled by Quadera® software. Following the same procedure several CO-H_2 pulses were alternatively flowed through the reactor, in order to study CO/ H_2 oxidation competition.

It should be mentioned that these experiments do not correspond to purely Oxygen Storage Capacity (OSCC and OSC) measurements as proposed by Duprez et al. [22] but tries to simulate the oxygen availability of the solid under the PrOx conditions.

2.3 Catalytic activity

The preferential CO oxidation reaction was carried out at atmospheric pressure in a stainless steel fixed bed reactor of 9 mm inner diameter, with a 100 mL.min^{-1} reaction feed composed by 1% CO, 1.5% O_2, 10% H_2O, 10% CO_2, 50% H_2 and N_2 as balance. For the hydrogen combustion CO was removed from the stream (1.5% O_2, 10% H_2O, 10% CO_2, 50% H_2 balanced in N_2) and for the direct CO oxidation H_2 was not included (1% CO, 1.5% O_2, 10% H_2O, 10% CO_2 balanced in N_2). The catalysts (100 mg, $100 < \phi < 200$ μm) were diluted with crushed glass particles with the same particle size forming a bed of about 5 mm in length. Products and reactants were separated and quantified by on-line gas chromatography (Agilent® 6890) equipped with HP PLOT Q and HP-5 columns and TCD detector. Prior the catalytic measurements, the samples were treated under a 100 $mL.min^{-1}$ flow of air, at 300ºC during 1 h.

The CO conversion was calculated according eq. (1) where CO_{in} is the inlet CO concentration and CO_{out} is the one at the outlet:

$$CO\ conversion\ (\%) = \frac{CO_{in} - CO_{out}}{CO_{in}} x100 \qquad (1)$$

The selectivity towards CO_2 formation was calculated using eq. (2). O_{2in} corresponds to oxygen in the inlet and O_{2out} to the one at the outlet.

$$selectivity\ (\%) = \frac{(CO_{in} - CO_{out})x100}{2\ x\ (O_{2in -}\ O_{2out})} \qquad (2)$$

In the CO-PrOx experiments presented in this study, λ parameter, eq. (3) was fixed at 3:

$$\lambda = \frac{2[O_2]}{[CO]} \qquad (3)$$

3. Results and discussion

Careful analysis of the catalyst properties of a material often starts with an exhaustive analysis of its electronic and redox properties. Regarding the complexity of the series of catalysts chosen in this study a separation between bi- and tri-component catalysts will be often considered for better description of the systems. In all the cases the alumina component will be neglected pointing to its principal role of metal oxide (CeO_2, CoO_x or mixed) dispersion and stabilization. This complex catalytic system is chosen consciously in order to obtain all type of possible interaction between components, e.g. electronic and redox, thus reflecting on the oxidation behavior of the catalysts.

Chemical composition and textural properties

Chemical composition and specific surface area of the prepared catalysts are presented in table 1. All the systems contain cerium oxide loadings close to the nominal value (15 wt. %). However, the impregnation of the cobalt spinel oxide on alumina results in important cobalt loss during the nitrate to hydroxides conversion, assigned to soluble amino cobalt complexes formation. The same was noticed for the cobalt-cerium mixed oxides, where only 50 % of the Co_3O_4 intended value was obtained. Gold deposition does not change further the catalysts composition. Contrary to the cobalt oxide loadings, the gold contents are very close to 2 wt%, and the gold deposition was successfully achieved.

X-Ray diffraction

XRD patterns of the supports are shown in Figure 1A. For every support, the XRD pattern shows diffraction lines corresponding to cubic CeO_2 fluorite type structure (JCPDS# 00-004-0593) and γ-Al_2O_3 phase (JCPDS# 00-048-0367). No signals due to crystalline cobalt oxides species were found. The low loadings of cobalt spinel, its high dispersion, and/or amorphous character may account for this fact. No ceria-cobalt solid solution formation was detected.

The diffraction patterns of the gold catalysts are shown in Figure 1B. All the systems manifest similar XRD diagrams. No signals due to metallic gold were detected indicating that gold particles are small (or at least beyond the detection limit of 4 nm) and well dispersed on the support.

Transmission electron microscopy

Selected TEM images of the gold catalysts are shown in Figure 2. A typical HAADF of the sample is presented in Figure 2A. The white spots correspond to the presence of heavier elements, such as Ce or Au. No clear differences in distribution, size and shape are evidenced among the catalysts. Gold particles are regularly distributed on the support surface with particle size ranging from 2 to 5 nm in good agreement with the XRD data. However, we must take into account that the very close atomic weight of cerium and gold makes their differentiation difficult due to the low mass and diffraction contrast. The high resolution TEM image presented in Figure 2B allows a better observation of the system. The gold nanoparticles appear always associated with cerium atoms as obtained by EDX analysis (not shown). This preferential precipitation of gold over ceria was reported and ascribed by Centeno et al. [23] to the strongest basic character of CeO_2 compared to alumina. The fact that the Ce is less electronegative than Co and Al, converts the Ce- bonded oxide ions in more basic type ligands, attracting the electron deficient gold atoms.

UV-Vis spectroscopy

UV-vis spectra of the prepared supports are presented in Figure 3A. Relevant information regarding the nature of the samples can be extracted from the spectra interpretation. First, several broad peaks appear in the 410-650 nm zone related to the presence of Co_3O_4 as was reported by Tsoncheva et al. [24]. A well resolved triplet with maxima at around 534, 581 and 630 nm and shoulders at around 455 and 700 nm are identified after a careful analysis of the spectra (Figure 3B). The triplet could be attributed to $4A_2(F)$ -- $T_1(P)$ transitions of Co^{2+} ions in tetrahedral oxygen coordination, while the shoulders at 430 and 720 nm are due to the formation of small amount of spinel Co_3O_4 phase. The appearance of this triplet of bands in the UV–vis spectra is generally taken as evidence of the formation of amorphous Co_3O_4 phase [25]. The amorphous character of this phase could explain the absence of cobalt oxide reflections in the XRD.

On the other hand, the broad band situated at about 350 nm in the UV region accounts for the ceria UV-vis features. This band is due to the charge transfer from 2p valence band of O^{2-} to 4f band of Ce^{4+} [25]. For ternary Ce-Co-Al systems, widening and shifting towards higher wavelengths of the absorption edge is observed evidencing Ce-Co interaction. The ceria band gap is estimated by plotting $[(F(R)h\nu]^{1/2}$ against energy and the linear part of the curve further extrapolated to $[(F(R)h\nu]^{1/2} = 0$. The results are summarized in Table 2. The direct band gap for the Ce/Al solid is very close to the reported value in the literature for a similar system [26]. A decrease of the band gap is observed for the Co-doped samples compare to the unmodified Ce/Al. This effect was previously observed and attributed to the fluctuation of the potential energy caused by the spatial dependence of the local density of states in doped semiconductors [27]. In terms of crystal field theory, Co^{3+} is a low spin species which possess d orbitals available for back-bonding interaction. In our case, the band gap shortening could be attributed to the cobalt oxide unoccupied lower energy orbitals supply, which decreases the energy needed for the $O^{2-} \rightarrow Ce^{4+}$ LUMO transitions.

The diffuse reflectance spectra of the gold catalysts are presented on Figure 3C. For all the samples, a new broad absorption band is observed in the range 500-570 nm. This contribution is assigned to the plasmon resonance of gold nanoparticles. For the Au/CeCoX/Al samples, the gold plasmon masks the cobal spinel bands. However, only remain visible for the Au/Co/Al sample. In addition, a shift of the ceria absorption edge provoked by the gold deposition is also observed. It should be noted that this shift is more marked than the one caused by the addition of cobalt oxide to the bare Ce/Al support. The later denotes that the Au-Ce interaction is stronger and more relevant than the Ce-Co interaction in terms of modification of the ceria electronic properties. Unfortunately, the gold plasmon difficults the band gap calculation but the strong metal-support interaction is foreseen from the spectra, and suggesting an electron rich Au/metal oxide interface, a site able to interact with the adsorbates during the reaction.

Reducibility: H_2-TPR

The reduction profiles of the solids under hydrogen are presented in Figure 4A. The Ce/Al presents only one reduction zone at around 495ºC attributed to the Ce^{4+} to Ce^{3+} reduction of the superficial ceria. The reducibility of pure and mixed cobalt oxides have been broadly studied [28-30]. For example, Sexton et al. [30] found that the reduction profile of Co_3O_4 consist of a low-temperature zone at around 300°C and a high-temperature zone between 300 and 700 °C, corresponding to the following processes:

$$Co_3O_4 \rightarrow CoO \rightarrow Co$$

For the Co/Al sample, it seems that the first reduction step occurs in a broad temperature range from 70 up to 500ºC while the second process takes place in much narrower zone (550-700ºC). For the Ce-Co mixed systems, the addition of cobalt shifts the reduction temperature of CeO_2. In spite of the fact that the observed reduction process is mainly related to ceria (due to the small fraction of Co in the sample) some cobalt oxide reduction is intended since a shoulder in the main reduction zone appeared. This shoulder becomes more important with the cobalt loading. In any case, cobalt and ceria reductions cannot be separated since they occur simultaneously, although apparently cobalt facilitates ceria reduction.

Regarding the gold catalysts, the noble metal addition helps even more by facilitating the mobility of H_2 on the surface of the solid. Au/Ce/Al sample shows two reduction zones, a low temperature one (centered at 150ºC) assigned to the noble metal promoted ceria surface reduction and the high temperature reduction process ascribed to the ceria bulk reduction. The observed shifting of the reduction process towards lower temperatures compared to the Ce/Al solid agrees with previous reports [31]. Gold also promotes cobalt spinel reducibility. Not only decrease in the reduction temperature but also a new reduction process at high temperature appeared. The last process could be associated to the complete cobalt reduction to Co^0. Similar to the binary Ce/Al or Co/Al systems, the presence of gold on Ce-Co mixed materials also facilitates the reduction of the mixed oxides and splits the reduction profile in several zones. Again ceria reduction is the predominant process to consider according to the catalysts composition. Nevertheless, cobalt reductive processes may contribute to the global catalyst reduction. In addition, the different Ce-Co interactions complicate the phenomena resulting in a complex TPR profile. To compare quantitatively the change in the reduction behavior of the support with the addition of the transition metal oxide or gold, the reduction percentage (RP) of every system was calculated according to the following equation:

$$RP = EHC/THC \times 100 \quad (4)$$

where THC is the theoretical hydrogen consumption (in moles) necessary for complete reduction of all reducible components of the corresponding sample, and EHC is the experimental hydrogen consumption measured during the TPR. For the RP calculation of the Co_3O_4 doped systems it is considered that the Ce and Co are present in their maximum oxidation state (Ce^{4+} and Co^{3+}), and both reduces from Co^{3+} to Co^0 and Ce^{4+} to Ce^{3+}. When gold is present in the samples, its reduction is discarded, and considered that the full reduction from Au^{3+} to Au^0 occurs during the calcination of the samples. RP values for all samples are presented in Figure 5.

The addition of cobalt to ceria increases the total reduction percentage. This effect is in line with the observed electronic Ce-Co interaction commented in the UV-Vis discussion. Indeed, as a result of the Ce-Co contact, the CeCo2/Al material is the support with the highest reducibility. All the gold catalysts presented higher reduction percentage than their parent supports. In should be mentioned that complete reduction was achieved for the Au/Co/Al and the Au/CeCo2/Al catalysts. Considering the temperature of PrOx reaction operation and its reductive atmosphere, an important degree of reduction is expected for the tested catalysts depending on its composition. Co potentiates Ce reduction and Au enhances both metal oxides reductive processes, pointing to easier oxygen mobility within the tri-component solid. This mobility could play a major role in the PrOx reaction and could be easily deduced with some oxygen storage experiences.

Oxygen Storage Capacity

The oxygen storage complete capacity (OSCC) provides information about the maximum reducibility of the samples while the oxygen storage capacity (OSC) informs about the most reactive and most available oxygen atoms [22]. It has to be indicated that these measurements have not been carried out under conventional conditions. Herein, a simulation of the PrOx atmosphere is pretended by using a series of H_2 pulses to saturate the surface before the CO treatments. More precisely, these measurements will give information on the reduction state of the catalysts under reaction stream. The OSCC measurements, expressed as the sum of the μmol CO_2 formed in each CO pulse, at the selected temperatures are presented in Table 3. As a general trend, the increase of the temperature from 90 ºC to 150 ºC increases the OSCC value for all the studied materials. For the binary solids, both Ce/Al and Co/Al some participation of their oxygen layers is detected even at temperatures as low as 90 ºC. The addition of Co to ceria increases slightly the available oxygen, either by increase of its mobility or by directly summing its oxygen layers. The gold containing samples presented much higher OSCC than their parent supports. The addition of gold promotes the support reducibility in good agreement with the TPR data. In order to find out the number of oxygen layers involved in the CO oxidation process, the measurements of the OSC were carried out. For the OSC theoretical calculations, the number of surface oxygen atoms and the BET area of each sample are considered. Also some assumptions are made, concretely: i) only oxygen atoms bonded to cerium participate in the oxygen storage process; ii) the surface is considered homogeneous iii) only one of four oxygen atoms is involved in the storage ($2CeO_2 \rightarrow Ce_2O_3$ + “O”) and iv) null gold metal contribution to the reduction, e.g. the gold metal could not be reoxidized. The same assumptions were established for the Co/Al and Au/Co/Al materials but all four oxygen atoms are implicated in the process ($Co_3O_4 \rightarrow 3Co$ + 4“O”) as proposed elsewhere [32]. The results are summarized in Table 3. For the supports, very small oxygen mobility was found at the studied temperatures. However, the addition of gold changes dramatically the oxygen mobility in the whole temperature range. The Au/Co/Al presents the highest number of available oxygen layers. For the Ce containing systems the ternary systems present an increase in the oxygen availability, especially at the lowest temperature, where the increase is considerable in comparison to the supports. In any case, fairly good oxygen mobility was found for all catalysts at the temperature of the reaction (90 and 150ºC) being the Au/Co/Al sample the highest oxygen provider. The ceria containing samples also present fairly well oxygen mobility. No matter the temperature almost two oxygen layers are implied in the CO oxidation.

CO/H_2 oxidation

Following the initial aim of this study, to verify if the H_2 oxidation activity is an useful criteria for PrOx catalysts selection, both CO and H_2 oxidation processes were separately investigated (Figures 6 and 7) in simulated post reforming stream (including H_2O and CO_2). Because of the large error in the quantification of water and the small change in hydrogen concentration due to the large excess of this compound, oxygen conversion was selected to express the H_2 combustion activity (Figure 6). Valuable information can be extracted from this plot. Firstly, hydrogen oxidation seems to be related to the presence of cobalt, since Co/Al and Au/Co/Al samples are the most efficient systems. Apparently the hydrogen oxidation activity increases with the number of oxygen layer involved in the process. Secondly, the ceria containing supports are more active in the hydrogen oxidation at low temperature range in comparison to their parent gold catalysts. Assuming that normally hydrogen is not chemisorbed on gold surfaces [29], the H_2 activation should then happen mainly on the support, probably on its structural defects such as oxygen vacancies. On the other hand, these oxygen vacancies are considered as preferential gold nucleation sites [14]. Hence, it could be expected, that in the gold samples these defects are already occupied by the gold nanoparticles which avoids the hydrogen adsorption and subsequent activation. Nevertheless, the decrease of the number of vacancies suppresses entirely the H_2 oxidation then this phenomenon does not take place on the supports, where the oxygen vacancies are available for the H_2 activation. The activity of the gold catalysts increased very quickly with the temperature, which is not surprising taking into account that the concentration of the oxygen vacancies also increases, following a potential Arrhenius-like behavior and the activation barrier for H_2 splitting is easily attained. Contrary to the results presented by Rossignol et al. [19], our results point that the support clearly plays a role in the hydrogen oxidation process. It is clear that the cobalt containing samples are more efficient in the hydrogen combustion and therefore, they are expected to be less selective in the PrOx reaction. Those samples show also the highest reducibility, which indicates that the high oxygen mobility increases preferably the H_2 oxidation.

CO oxidation in the presence of CO_2 and H_2O was also evaluated and the results are presented in Figure 7. For both, supports and gold catalysts, the catalytic activity follows the sequence: CeCo2/Al > CeCo1/Al > Ce/Al > Co/Al. The Ce-Co mixed systems resulted to be the most active within the series evidencing that cobalt to ceria promotion leads to increase of the rate of carbon monoxide oxidation more rapidly than H_2 oxidation. Considering the catalyst's properties these solids present the highest Ce containing interface which appears to be more important for the CO oxidation than purely the oxygen mobility. This is confirmed also by the fact that the adding of gold does not change the tendency of activity only increases it considerably. The Au/CeCo/Al mixed samples showed higher activity in the CO oxidation reaction. Contrary to the H_2 oxidation experiment, the Au/Co/Al sample shows the lowest activity in the CO oxidation highlighting the need of ceria containing interface to achieve good activity in the carbon monoxide combustion. One point should be underlined here, the notorious effect of the CO_2 and H_2O presence in the CO oxidation activity for those samples. In a conventional CO oxidation test (mixing only CO + O_2), these samples can achieve total conversion even at sub-ambient temperatures as published elsewhere for similar series of catalysts [16]. It is reported, that the presence of steam in the reactant mixture inhibits the CO oxidation reaction [33, 34, 35]. The presence of CO_2 also could inhibit the CO oxidation reaction, by its slow rate of desorption from the surface and active sites blocking on the catalyst surface.

For further comprehension of the competition between CO and H_2 oxidation reactions and the role played by the support in these processes, several pulse experiments were considered. The most active sample Au/CeCo2/Al and its corresponding support CeCo2/Al have been selected for this study at two relevant temperatures in the PrOx reaction. Various points are worth to consider regarding these results. At 90ºC the Au/CeCo2/Al catalyst (Figure 8A) showed activity in the CO oxidation which is in concordance with the activity data presented in Figure 7. Every pulse of CO produces a CO_2 signal accounting for the activity of the surface oxygen. It was also observed that the CO_2 signals have two components that may indicate the presence of two CO oxidation processes. Furthermore, the second CO oxidation process seems to become more important with time since its contribution grows with every successive pulse. It should be underlined that these measurements are carried out in the absence of oxygen, so the oxygen involved in the CO oxidation processes is provided only by the support. The later indirectly gives information about the oxygen storage capacity of the samples. Here again it is evidenced that the addition of gold promotes the support ability to provide oxygen or, at least, when gold is present, the available oxygen is more labile and reacts more quickly. For the same sample, when the temperature was increased up to 150ºC (Figure 8 B) a decrease in the CO oxidation activity was noticed. The later could be associated to the support reduction and its impossibility to be reoxidized in the conditions of the treatment (by the 10 O_2 pulses between the change of the temperature). In any case, these data confirm that CO oxidation in this particular catalyst is favored at low temperature and hydrogen oxidation become relevant when the temperature is increased, thus decreasing the selectivity. It seems that at 90ºC, when the surface is saturated with H_2, CO is able to displace H_2 from the surface and reach the actives sites of the catalyst and subsequently react. However, this ability of CO to remove hydrogen from the catalyst surface decreases with the temperature and therefore the CO oxidation diminishes in favor of the hydrogen oxidation marking the selectivity of the preferential CO oxidation.

The behavior of the CeCo2/Al sample is also interesting. Figure 8C shows the pulses experiment for this sample at 90ºC. No activity in the CO oxidation is found at this temperature. Nevertheless, a high amount of water was formed after each hydrogen pulse accounting for the activity in the H_2 combustion. The oxygen of the support is devoted to H_2 oxidation instead of CO oxidation. In other words, H_2 combustion is mainly related to the support, especially at low temperatures. This result totally agrees with the activity data presented above. The supports are definitely more active than the gold samples for the H_2 combustion at low temperatures. When the temperature is increased (Figure 8D), some CO oxidation activity is detected. Once again, this result correlates with the activity in the CO oxidation discussed above. It is important to underline that, while for the gold based system two CO oxidation processes were found, here only one CO_2 signal is obtained. Moreover, if we compare Figures 8A and 8D, it can be noticed that the second CO oxidation reaction observed in the gold catalysts seems to be the same that the observed for the support. The later means that the support also assists the CO oxidation activity of the gold based catalysts. The first and more rapid CO oxidation reaction is probably related to the gold nanoparticles and/or gold/support interface and the second one to the support interface, in this case Co/Ce one.

PrOx complete study

The CO oxidation ability in the presence of hydrogen of the prepared materials is studied over both, gold based catalyst and their corresponding supports. The activity of the supports is presented in Figure 9A. The observed CO conversion follows the next activity order:

Co/Al > Ce/Al > CeCo2/Al ~ CeCo1/Al

Contrary to the CO oxidation in absence of H_2 the best catalytic performance exhibits the Co/Al sample. The CO oxidation for Co-containing systems is reported to follow a redox cycle where CO is absorbed on a cobalt site and subsequently reacts with lattice oxygen to form CO_2 and an oxygen vacancy [33]. In the next step, this oxygen vacancy is replenished by the water in the stream. In other words, water reoxidizes the surface to complete the cycle. Nevertheless, the presence of a high amount of hydrogen in the PrOx reaction limits the oxidative properties of water thus decreasing the CO oxidation rate. The poorer activity of the CeCo/Al mixed samples compared to the Co/Al one can be related to the lower oxygen storage complete capacity of the ceria containing samples and to the less amount of surface O_2 available for the reaction. The number of available O_2 is then of primordial importance in the PrOx reaction over the supports, effect equal to that found for the H_2 oxidation. Higher the OSCC higher the H_2 oxidation and higher the PrOx activity.

The presence of gold, however, changes completely the picture. As shown by OSCC-OSC measurements, Au boosts the oxygen mobility and converts all samples in very effective catalysts for CO elimination. Although the presence of hydrogen was reported to mitigate the support effect in the PrOx reaction [19] in our study the presence of ceria, and more precisely, the cobalt to ceria promotion appears to be crucial for the better CO oxidation activity. This promotional effect for the Ce-Co mixed system could be attributed to the modification of ceria electronic redox properties as can be intended from the UV-Vis and the increase of the Ce/Co interface responsible for CO oxidation. Therefore, electron transfer reaction such as CO oxidation would proceed easier in the promoted materials in good agreement with our CO-PrOx data. The Au/CeCo2/Al sample resulted to be the most efficient catalyst in the whole temperature range.

Examining the selectivity data presented in Figure 10 A it could be observed that none of the studied samples showed high selectivity values. The shape of the plot is similar for all the catalysts, higher the temperature, lower the selectivity towards CO oxidation. In view of the oxygen conversion data (Figure 10B) for lambda value of 3 (amount of oxygen in stream three times the stoichiometrically needed) the maximum oxygen conversion should be 33 % if only CO is oxidized. However 100 % of O_2 conversion is achieved for all the systems indicating that H_2 combustion occurs in the whole temperature range.

The comparison between the CO oxidation tests (Figure 7) and the CO-PrOx ones (Figure 9) is also worthy to consider. For the supports the activity increases with the temperature irrespectively to the presence of H_2 in the stream. For the gold catalysts CO oxidation activity increases with the temperature reaching total conversion in the best case, however the shape of the CO-PrOx curve is different. The activity increased with the temperature till a critical point (130-150ºC) where hydrogen oxidation becomes dominant and the CO oxidation yield falls. This temperature range marks the change in the selectivity of the reaction, as evidenced previously in the pulse experiment. It is clear that at low temperatures the presence of hydrogen is beneficial for the CO oxidation activity, an effect also reported by Quinet et al. [36, 37]. It seems that the CO PrOx reaction proceeds via the reaction of Au bonded CO with hydroperoxy (OOH) intermediates originating from H_2 oxidation on gold surface [38]. Ironically, a good gold based

CO-PrOx catalyst should possess activity in both H_2 and CO oxidation simultaneously. The undesirable H_2 combustion cannot be avoided when gold based systems are employed in the PrOx reaction due to the intrinsic activity of gold to catalyze this process. Nevertheless, as evidenced in this paper, a fairly good control of the hydrogen combustion could be obtained by the proper choice of the support, since the support is directly involved in this process exhibiting even higher H_2 oxidation activity than the gold based catalysts at low temperatures. Therefore, the catalytic screening in the H_2 oxidation is an easy and recommendable test that must be considered for the optimum catalysts selection. Higher the OSCC of the support higher the H_2 oxidation and lower the selectivity in PrOx. For this series of catalyst higher the Ce/metal interface higher the CO oxidation.

4. Conclusions

A series of effective CO-PrOx catalysts based on $Au/CeO_2/Al_2O_3$ catalytic formulation has been developed. The inclusion of small amounts of cobalt oxide on the catalyst formula appreciably improves the CO-PrOx oxidation activity in a real post-reforming stream, being the Ce-Co mixed samples the most performing ones. The Ce-Co contact results in satisfactory electronic and redox properties, especially enhanced OSC that benefits the catalytic activity.

The combustion of H_2 mainly occurs on the support, thus a strong support effect on the H_2 combustion activity has been found. The later means that the hydrogen oxidation capacity of a gold based system can be modulated with a proper support choice in order to obtain the best activity/selectivity balance. A simple experiment like H_2 combustion in the post-reforming conditions could provide very useful information regarding the catalyst design for H_2 clean-up goals.

5. Acknowledgements

T.R. Reina acknowledges CSIC for his JAE-Predoc fellowship and S. Ivanova MEC for her Ramon y Cajal contract. The Spanish Ministerio de Ciencia e Innovación under contract ENE2012-374301-C03-01 and Junta de Andalucía under contract TEP-8196 provide financial support for this work, both programs are co-funded by the European Union FEDER. Dr J.J. Delgado is also kindly acknowledged for the TEM experiments.

6.References

[1] R.J. Farrauto, Appl. Catal. B: Env. 58 (2005) 3-7.

[2] F. Joensen, J. R. Rostrup-Niesen, J. of Power Sources 105 (2002) 195-201.

[3] D.L. Trim, Appl. Catal. A: Gen. 296 (2005) 1-11.

[4] V. Idakiev, T. Tabakova, K. Tenchev, Z.Y. Yuan, T.Z. Ren, B.L. Su, Catal. Today 128 (2007) 223-229.

[5] T. Tabakova, V. Idakiev, J. Papavasiliou, G. Avgouropoulos, T. Ioannides, Catal. Commun. 8 (2007) 101-106.

[6] Z.Y. Yuan, V. Idakiev, A. Vantomme, T. Tabakova, T.Z. Ren, B.L. Su, Catal. Today 131 (2008) 203-210.

[7] F. Mariño, G. Baronetti, M. Laborde, N. Bion, A. Le Valant, F. Epron, D. Duprez, Int. J. of Hydrog. Energy 33 (2008) 1345-1353.

[8] G. Avgouropoulos, T. Ioannides, Ch. Papadopoulou, J. Batista, S. Hocevar, H.K. Matralis, Catal. Today 3 (2002) 157-167.

[9] T. Tabakova, G. Avgouropoulos, J. Papavasiliou, M. Manzoli, F. Boccuzzi, K. Tenchev, F. Vindigni, T. Ioannides, App. Catal. B: Env 101 (2011) 256-265.

[10] M.M. Schubert, V. Plzak, J. Garche, R.J. Behm, Catal. Lett. 76 (2001) 143-150.

[11] W. Deng, J. De Jesus, H. Saltsburg, M. Flytzani-Stephanopoulos, Appl. Catal. A 291 (2005) 126-135.

[12] E. Ko, E.D. Park, K.W. Seo, H.C. Lee, D. Lee, S. Kim, Catal. Today 116 (2006) 377-383.

[13] G. Avgouropoulos, M. Manzoli, F. Boccuzzi, T. Tabakova, J. Papavasiliou, T. Ioannides, V. Idakiev, J. of Catal. 256 (2008) 237-247.

[14] O.H. Laguna, F. Romero-Sarria, M.A. Centeno, J.A. Odriozola, J. of Catal. 276 (2010) 360-370.

[15] W.Y. Hernández, M.A. Centeno, F. Romero-Sarria, J.A. Odriozola, J. of Phys. Chem. C 114 (2010) 10857- 10865.

[16] T.R. Reina, A. Álvarez, S. Ivanova, J.A. Odriozola, M.A. Centeno, ChemCatChem 4 (2012) 512-520.

[17] M. Okumura, S. Tsubota, M. Haruta, J. of Mol. Catal. A 199 (2003) 73-84.

[18] B. Schumacher, Y. Denkwitz, V. Plzak, M. Kinne, R.J. Behm, J. of Catal. 224 (2004) 449-462.

[19] C. Rossignol, S. Arrii, F. Morfin, L. Piccolo, V. Caps, J.L. Rousset, J. of Catal. 230 (2005) 476–483.

[20] R.J.H. Grisel, C.J. Weststrate, A. Goossens, M.W.J. Crajé, A.M. Van der Kraan, B.E. Nieuwenhuys, Catal. Today 72 (2002) 123-132.

[21] S. Ivanova, C. Petit, V. Pitchon, Appl. Catal. A: Gen. 267 (2004) 191-201.

[22] S. Kacimi, J. Barbier, R. Taha, D. Duprez, Catal. Lett. 22 (1993) 343–350.

[23] M.A. Centeno, Portales, I. Carriozosa, J.A. Odriozola, Catal. Lett. 102 (2005) 289-296.

[24] T. Tsoncheva, A. Gallo, N. Scotti, M. Dimitrov, R. Delaigle, E.M. Gaigneaux, D. Kovacheva, V. Dal Santo, N. Ravasio, Appl. Catal. A: Gen. 417 (2012) 209-219.

[25] S. Esposito, M. Turco, G. Ramis, G. Bagnasco, P. Perniced, C. Pagliuca, M. Bevilacqua, A. Aronned, J. of Solid State Chem. 12 (2007) 3341-3350.

[26] M.A. Centeno, M. Paulis, M. Montes, J.A. Odriozola, Appl. Catal. A: Gen. 234 (2002) 65-78.

[27] T. Dhannia, S. Jayalekshmi, M.C. Santhosh Kumar, T. Prasada Rao, A. Chandra Bose, J. of Phys. Chem. Solids 71 (2010) 1020-1028.

[28] H.Y. Lin, Y.W. Chen, C. Li, Thermochimica Acta 400 (2003) 61-67.

[29] H.Y. Lin, Y.W. Chen, Mater. Chem. and Phys. 85 (2004) 171-175

[30] B.A. Sexton, A.E. Hughes, T.W. Turney, J. of Catal. 97 (1986) 390-406

[31] G. Jacobs, E. Chenu, P.M. Patterson, L. Williams, D. Sparks, G. Thomas, B.H. Davis, Appl. Catal. A 258 (2004) 203-214.

[32] A. Alvarez, S. Ivanova, M.A. Centeno, J.A. Odriozola, Appl. Catal. A: Gen. 431-432 (2012) 9-17.

[33] M. Haruta, S. Tsubota, T. Kobayashi, H. Kageyama, M.J. Genet, B.J. Delmon, J. of Catal. 144 (1993) 175-192.

[34] S. Royer, D. Duprez, ChemCatChem 3 (2011) 24–65.

[35] D.A.H. Cunningham, T. Kobayashi, N. Kamijo, M. Haruta, Catal. Lett. 25 (1994) 257-264.

[36] E. Quinet, L. Piccolo, F. Morfin, P. Avenier, F. Diehl, V. Caps, J.L. Rousset, J. of Catal. 268 (2009) 384-389.

[37] E. Quinet, L. Piccolo, H. Daly, F. Meunier, F. Morfin, A. Valcarcel, F. Diehl, P. Avenier, V. Caps, J.L. Rousset Catal. Today 138 (2008) 43-49.

[38] L. Piccolo, H. Daly, A. Valcarcel, F. Meunier, Appl. Catal. B: Env. 86 (2009) 190-195.

Figure 1: XRD patterns of the prepared samples; A) supports; B) gold catalysts.

Figure 2: Selected TEM micrographs of the Au/Ce/Al catalyst; A) HAADF; B) HRTEM.

Figure 3: Diffuse reflectance spectra A) supports; B) supports region 400-700 nm; C) gold catalysts.

Figure 4: TPR-H_2 profiles of the supports (full lines) and their corresponding gold catalysts (dashed lines); A) binary systems; B) Ce-Co ternary systems.

Figure 5: Reduction percentage for the studied solids.

Figure 6: H_2 oxidation activity of the prepared materials (gas mixture: 1.5% O_2, 50%H_2, 10%H_2O, 10%CO_2 balanced in N_2).

Figure 7: CO oxidation activity of the prepared materials A) supports B) gold catalysts (gas mixture: 1.5% O_2, 1% CO, 10%H_2O, 10%CO_2 balanced in N_2).

Figure 8 CO/H_2 pulses A) Au/CeCo2/Al at 90ºC B) Au/CeCo2/Al at 150ºC C) CeCo2/Al at 90ºC D) CeCo2/Al at 150ºC .

Figure 9 Catalytic activity in the PrOx reaction A) supports; B) Gold catalysts.

Figure 10: Selectivity of the gold catalysts in the PrOx reaction B) O_2 conversion of the gold catalysts in the PrOx reaction.

Table 1: Chemical composition and surface area of the synthesized samples

Sample	CeO_2 (wt.%)	Co_3O_4 (wt.%)	Au (wt.%)	S_{BET} (m^2/g)
Al	-	-		202
Ce/Al	15.34	-	-	186
Co/Al		2.91	-	185
CeCo1/Al	14.68	0.43	-	202
CeCo2/Al	14.36	0.81	-	177
Au/Ce/Al	15.32	-	1.7	197
Au/Co/Al	-	2.86	2.05	194
Au/CeCo1/Al	14.39	0.42	2.17	195
Au/CeCo2/Al	13.71	0.77	2.03	174

Table 2: CeO_2 direct band gap of the prepared supports

sample	CeO_2 Direct band gap (eV)
Ce/Al	3.04
CeCo1/Al	2.94
CeCo2/Al	2.89

Table 3: Oxygen storage complete capacity (OSCC) and oxygen storage capacity (OSC) in µmol CO_2/g sample *at reaction conditions* and number of oxygen layers (NL), as a function of the temperature

Sample	$OSCC_{90°C}$	$OSCC_{150°C}$	$OSC_{90°C}$	$OSC_{150°C}$	$NL_{90°C}$	$NL_{150°C}$
Co/Al	24.3	28.6	3.25	5.10	0.06	0.09
Ce/Al	17.2	19.1	1.81	4.25	0.01	0.05
CeCo2/Al	19	20.12	2.52	10.61	0.02	0.07
Au/Co/Al	551	902	155	342	2.74	6.05
Au/Ce/Al	806	979	225	281	1.42	1.77
Au/CeCo2/Al	619	752	221	251	1.64	1.86

Figure 1

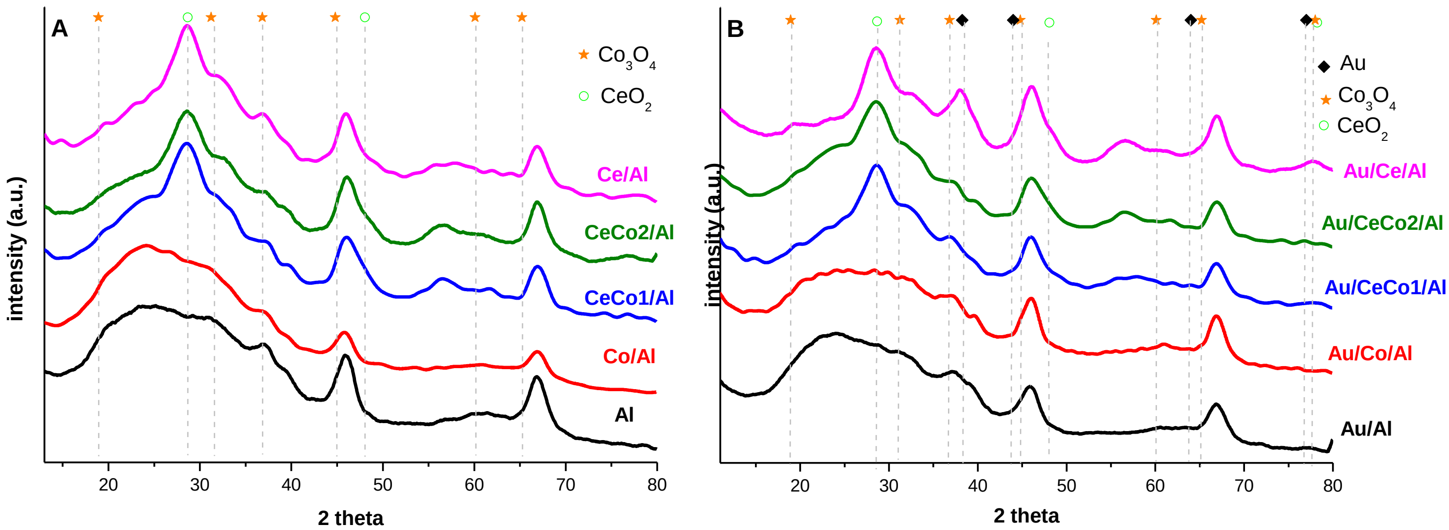
A
B
Co3O4
CeO2
Au
Ce/Al
CeCo2/Al
CeCo1/Al
Co/Al
Al
Au/Ce/Al
Au/CeCo2/Al
Au/CeCo1/Al
Au/Co/Al
Au/Al
intensity (a.u.)
2 theta
20
30
40
50
60
70
80

Figure 2

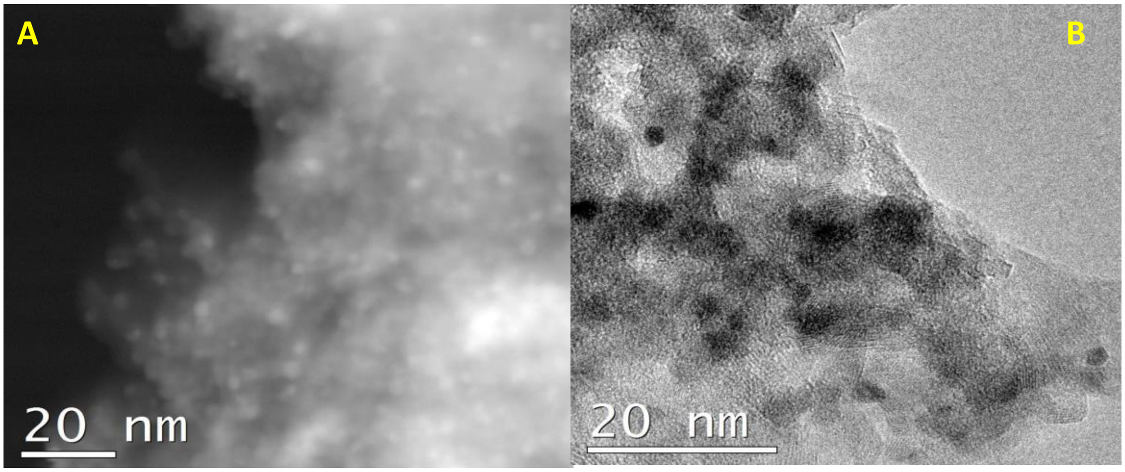

Figure 3

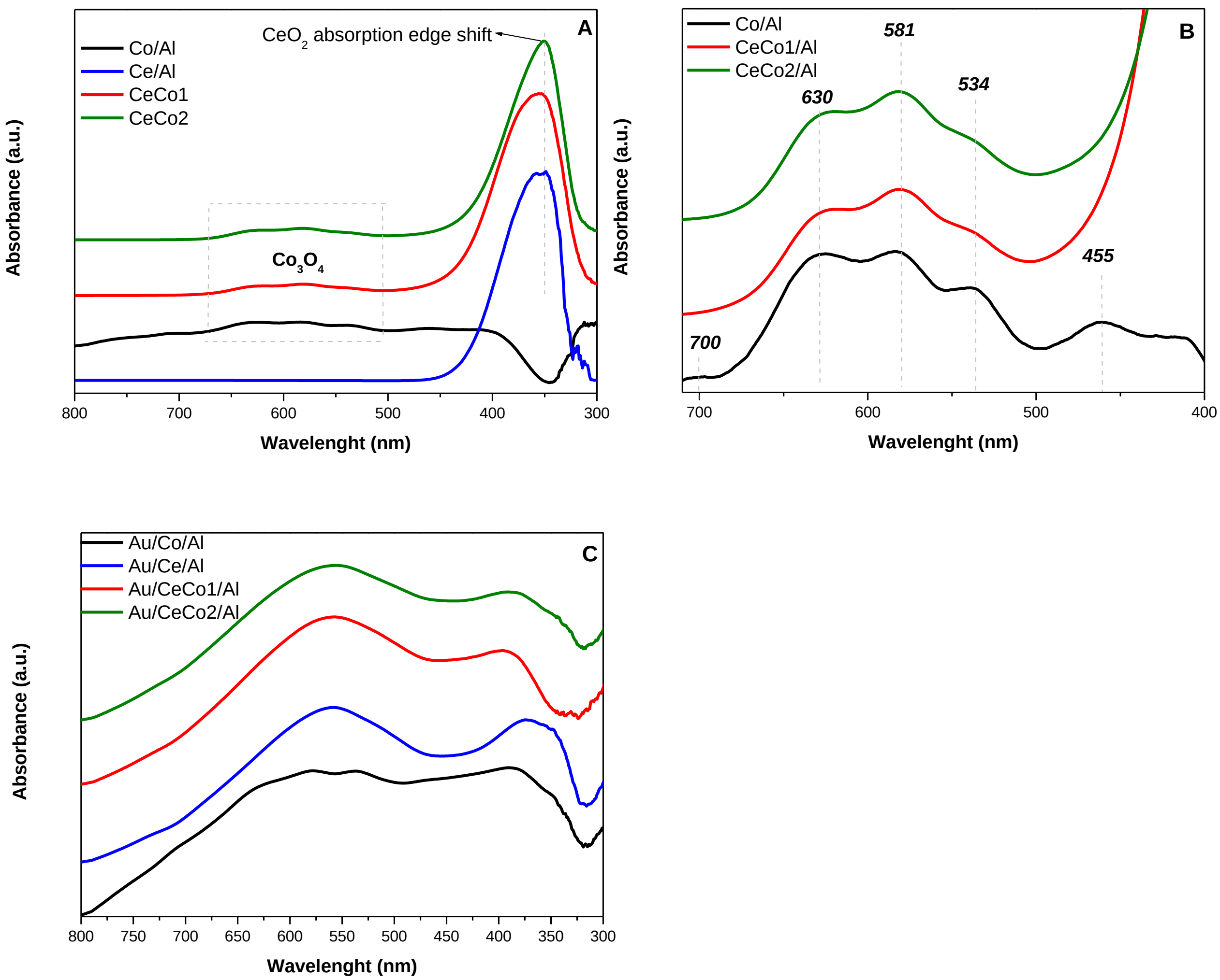

A
Co/Al
Ce/Al
CeCo1
CeCo2
CeO2 absorption edge shift
Co3O4
Absorbance (a.u.)
Wavelenght (nm)
800
700
600
500
400
300
B
Co/Al
CeCo1/Al
CeCo2/Al
581
630
534
455
700
Absorbance (a.u.)
Wavelenght (nm)
700
600
500
400
C
Au/Co/Al
Au/Ce/Al
Au/CeCo1/Al
Au/CeCo2/Al
Absorbance (a.u.)
Wavelenght (nm)
800
750
700
650
600
550
500
450
400
350
300

Figure 4

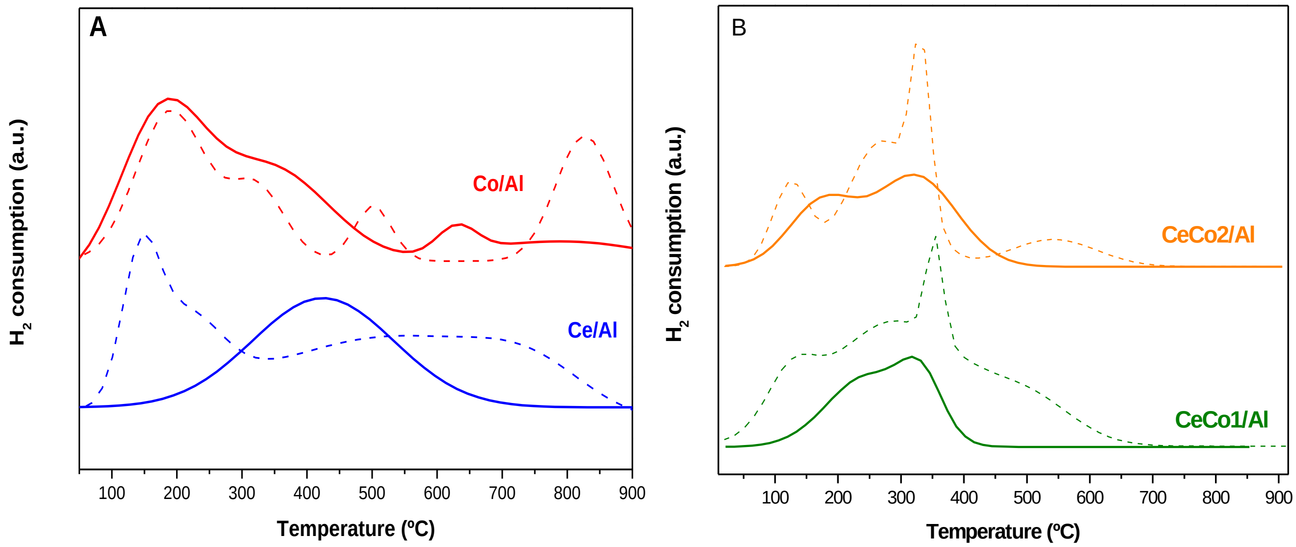
A
Co/Al
Ce/Al
H2 consumption (a.u.)
100 200 300 400 500 600 700 800 900
Temperature (ºC)
B
CeCo2/Al
CeCo1/Al
H2 consumption (a.u.)
100 200 300 400 500 600 700 800 900
Temperature (ºC)

Figure 5

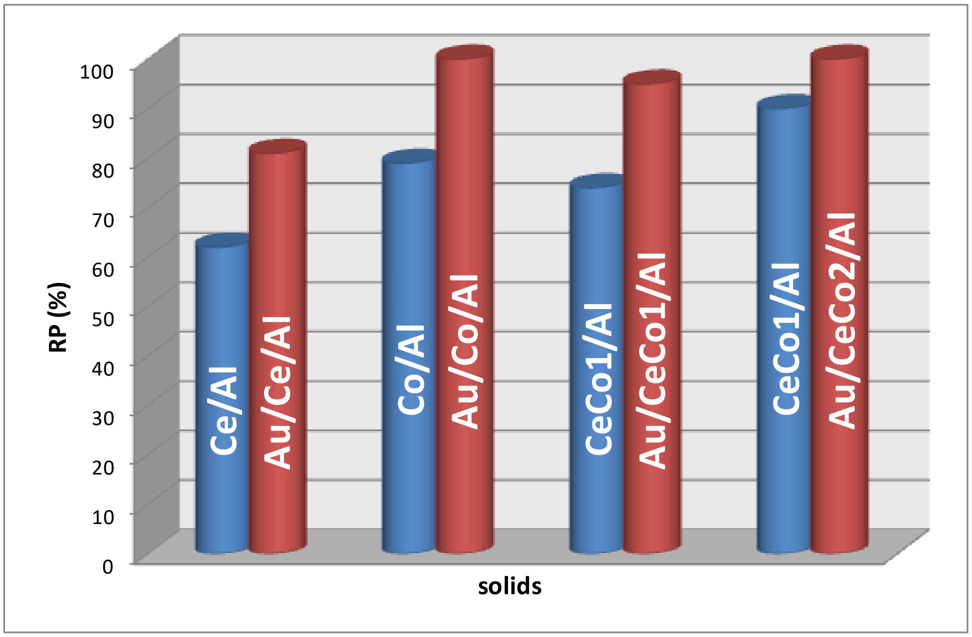
100
90
80
70
60
50
40
30
20
10
0
RP (%)
Ce/Al
Au/Ce/Al
Co/Al
Au/Co/Al
CeCo1/Al
Au/CeCo1/Al
CeCo1/Al
Au/CeCo2/Al
solids

Figure 6

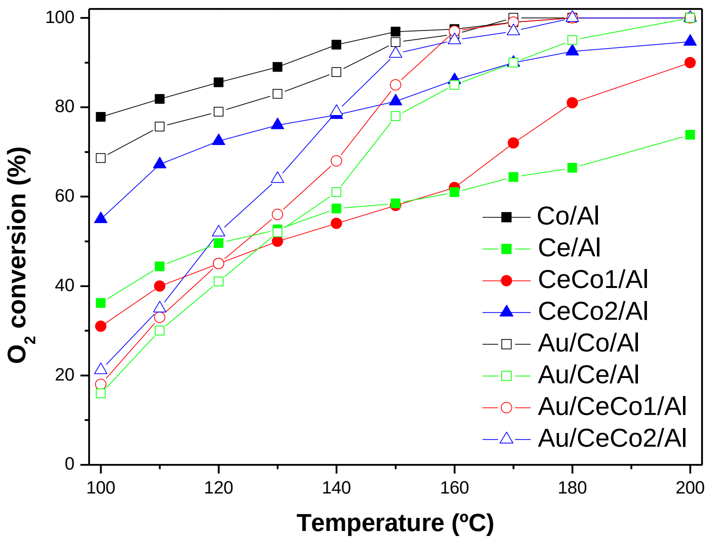

100
80
60
40
20
0
O_2 conversion (%)
100
120
140
160
180
200
Temperature (ºC)
Co/Al
Ce/Al
CeCo1/Al
CeCo2/Al
Au/Co/Al
Au/Ce/Al
Au/CeCo1/Al
Au/CeCo2/Al

Figure 7

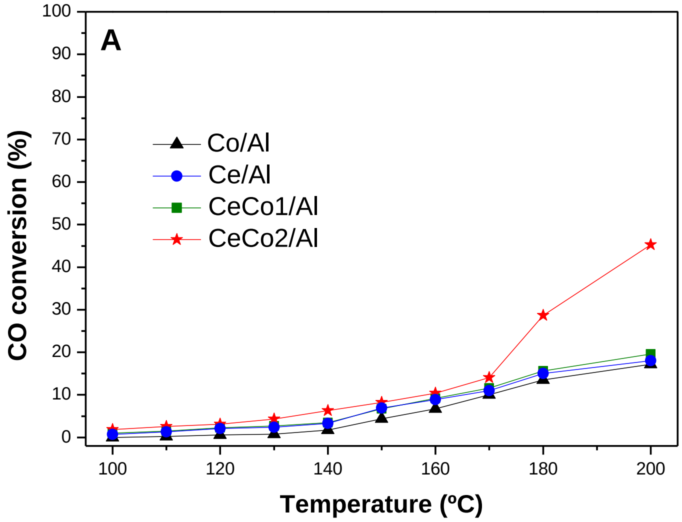

A
CO conversion (%)
Temperature (ºC)
Co/Al
Ce/Al
CeCo1/Al
CeCo2/Al
0
10
20
30
40
50
60
70
80
90
100
100
120
140
160
180
200

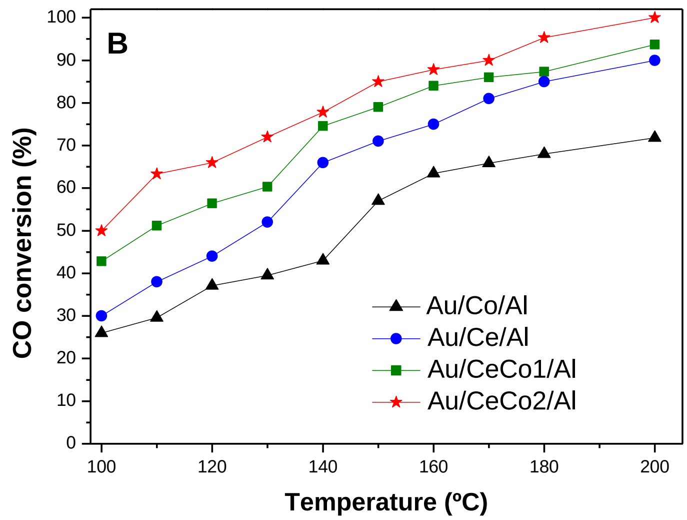

B
CO conversion (%)
Temperature (ºC)
Au/Co/Al
Au/Ce/Al
Au/CeCo1/Al
Au/CeCo2/Al
0
10
20
30
40
50
60
70
80
90
100
100
120
140
160
180
200

Figure 8

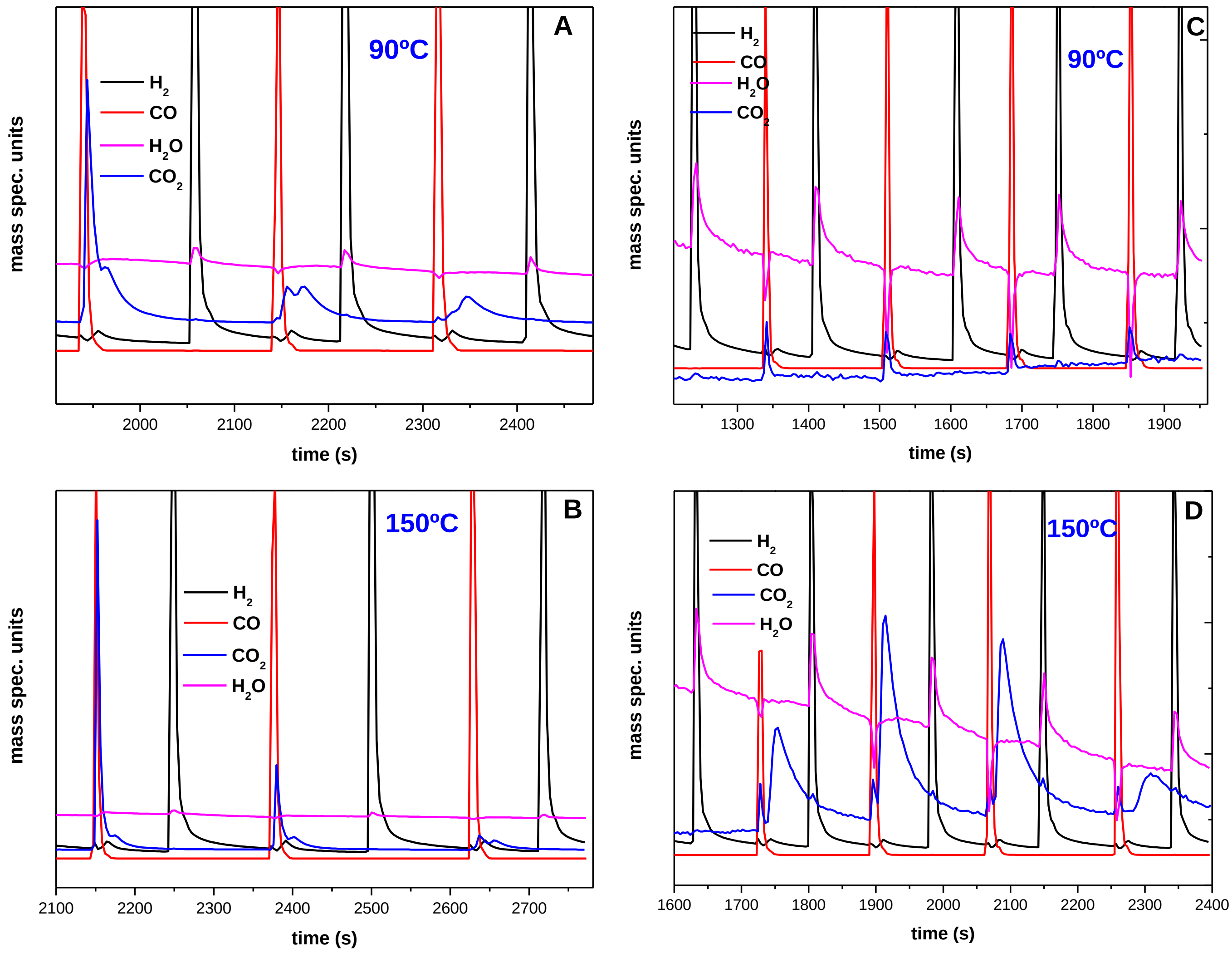

A
90ºC
H2
CO
H2O
CO2
mass spec. units
2000
2100
2200
2300
2400
time (s)
C
90ºC
H2
CO
H2O
CO2
mass spec. units
1300
1400
1500
1600
1700
1800
1900
time (s)
B
150ºC
H2
CO
CO2
H2O
mass spec. units
2100
2200
2300
2400
2500
2600
2700
time (s)
D
150ºC
H2
CO
CO2
H2O
mass spec. units
1600
1700
1800
1900
2000
2100
2200
2300
2400
time (s)

Figure 9

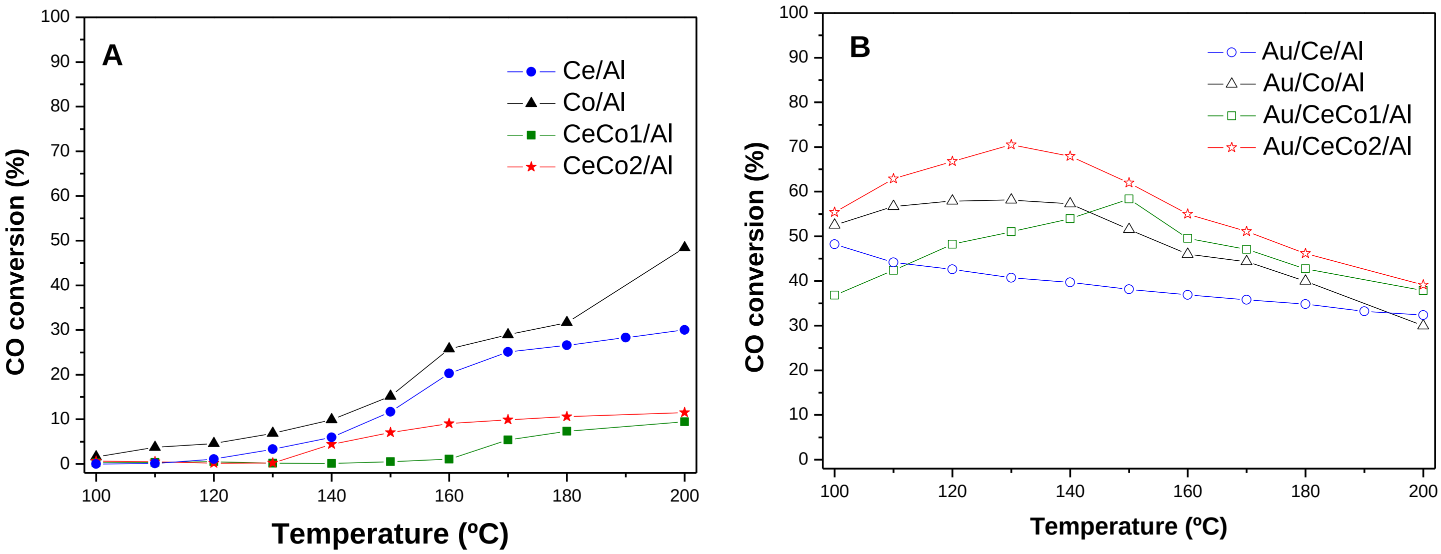

A
Ce/Al
Co/Al
CeCo1/Al
CeCo2/Al
CO conversion (%)
Temperature (ºC)
0
10
20
30
40
50
60
70
80
90
100
120
140
160
180
200
B
Au/Ce/Al
Au/Co/Al
Au/CeCo1/Al
Au/CeCo2/Al

Figure 10

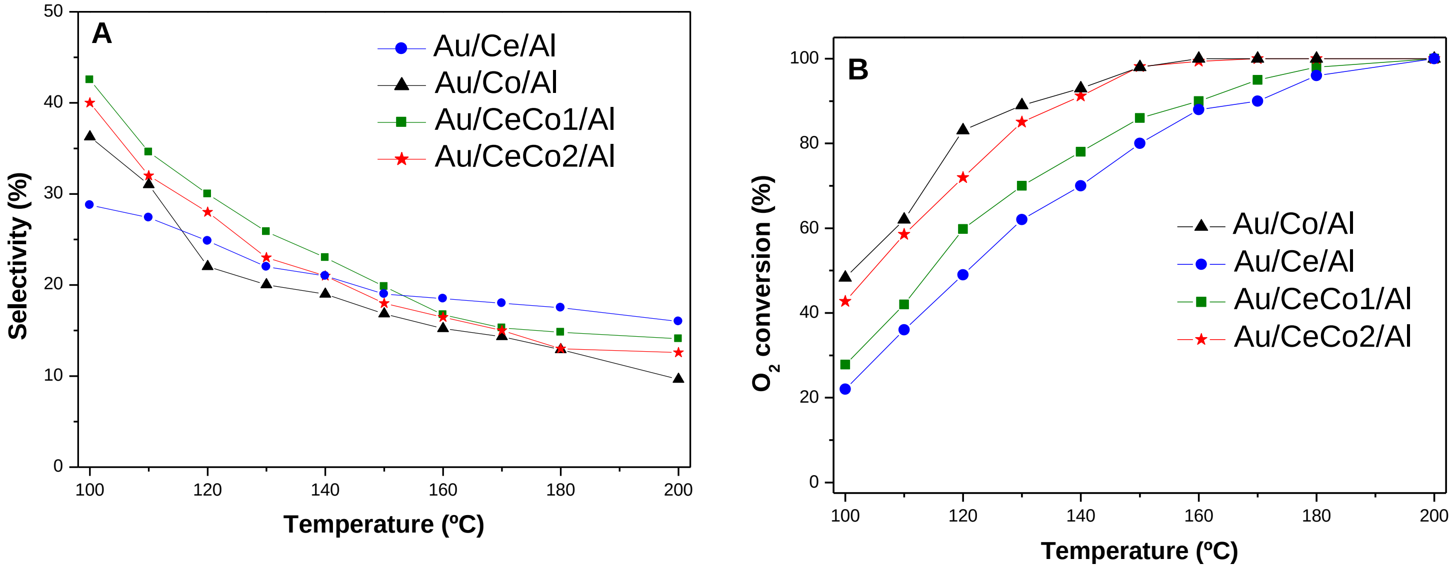
A
Au/Ce/Al
Au/Co/Al
Au/CeCo1/Al
Au/CeCo2/Al
Selectivity (%)
Temperature (ºC)
B
Au/Co/Al
Au/Ce/Al
Au/CeCo1/Al
Au/CeCo2/Al
O2 conversion (%)
Temperature (ºC)